*DOI:10.25092/baunfbed. 1538657* *J. BAUN Inst. Sci. Technol., 27(1), 297-314, (2025)*

# Synthesis, spectroscopic, crystal structure and DFT investigation of the Cu(II) complex with mixed 2,2'-dimethylmalonate/2,2'-bipyridine ligands

**Mustafa Serkan SOYLU***

*Giresun University, Faculty of Arts and Sciences, Department of Physics, Giresun.*

*Geliş Tarihi (Received Date): 26.08.2024*
*Kabul Tarihi (Accepted Date): 23.12.2024*

## Abstract

*In this study; a mixed ligand Cu(II) complex, [Cu($Me_2$mal)(bpy)($H_2O$)]·$H_2O$ ($Me_2mal^{-2}$= Dimethylmalonate dianion, bpy=2,2'-bipyridine) was synthesized and characterized experimentally and theoretically by IR, UV and single crystal X-ray diffraction. The complex crystallizes in the orthorhombic system with space group Pnnm. In the complex, the Cu center is coordinated by a $Me_2mal^{-2}$ dianion and a bpy molecule, and the $N_2O_2$ exhibits square-planar geometry. The axial position was occupied by the water molecule. The crystal packing of the complex is stabilized by O-H…O hydrogen bonds and π–π interactions. The contribution of hydrogen bonding and π–π stacking interactions to crystal packing was also investigated. Theoretical calculations using the DFT method were also carried out in this study. DFT (B3LYP/6-31G) and TD-DFT (B3LYP/LanL2DZ) calculation methods were used to obtain the geometric, vibrational and electronic properties of the synthesized complex and the obtained theoretical calculation results and experimental results are presented comparatively in this study.*

***Keywords:*** *Dimethylmalonate; Cu(II) Coordination Complex ; Quantum Chemical Computation ; Crystal Structure; IR ; UV-Vis.*

# Karışık 2,2'-dimetilmalonat/2,2'-bipiridin ligandlı Cu(II) kompleksinin sentezi, spektroskopik, kristal yapı ve DFT incelemesi

## Öz

*Bu çalışmada; karışık ligantlı Cu(II) kompleksi, [Cu($Me_2$mal)(bpy)($H_2O$)]·$H_2O$ ($Me_2mal^{-2}$= Dimetilmalonat dianyonu, bpy=2,2'-bipiridin) sentezlenmiştir. Sentezlenen kompleks*

*Mustafa Serkan Soylu, mustafa.serkan.soylu@giresun.edu.tr, https://orcid.org/0000-0002-8440-1260

*IR, UV ve tek kristal X-ışını kırınımı yöntemleri ile deneysel ve kuantum mekaniksel hesaplama yöntemleri kullanılarak teorik olarak karakterize edilmiştir. Kompleks, Pnnm uzay grubunda ortorombik kristal sisteminde kristallenmiştir. Komplekste Cu merkezi; bir $Me_2mal^{-2}$ dianyonu ve bir bpy molekülü tarafından koordine edilmiştir ve $N_2O_2$ kare-düzlemsel geometri sergilemektedir. Eksensel pozisyonda ise su molekülü bulunmaktadır. Kompleksin kristal paketlenmesi O-H...O hidrojen bağları ve π–π etkileşimleri ile kararlı bir yapı oluşturmuştur. Çalışmada hidrojen bağlarının ve π–π istifleme etkileşimlerinin kristal paketlenmeye katkısı da araştırılmıştır. Bu çalışmada DFT yöntemi kullanılarak teorik hesaplamalar da yapılmıştır. Sentezlenen kompleksin geometrik, titreşimsel ve elektronik özelliklerini elde etmek için DFT (B3LYP/6-31G) ve TD-DFT (B3LYP/LanL2DZ) hesaplama yöntemleri kullanılmıştır. Elde edilen teorik hesaplama sonuçları ve deneysel sonuçlar karşılaştırmalı olarak verilmiştir.*

***Anahtar kelimeler:*** *Dimetilmalonat; Cu(II) Koordinasyon Kompleksi; Kuantum Kimyasal Hesaplama; Kristal Yapı; IR; UV-Vis.*

## 1. Introduction

Transition metal complexes play a crucial role in the development of new functional materials due to their wide-ranging applications in catalysis, magnetism, luminescence, and molecular electronics. Among these, dicarboxylate ligands, particularly malonates and their derivatives, have attracted considerable attention owing to their versatile coordination behavior and potential to form stable, multidimensional frameworks. These ligands, characterized by their two carboxylate groups in a 1,3-position, enable diverse binding modes such as chelating bidentate and bridging coordination, thereby significantly expanding the structural diversity and functionality of the resulting metal complexes [1].

Dimethylmalonate ($Me_2mal^{2-}$), a derivative of malonic acid, is especially notable due to its structural rigidity, chemical stability, and ability to form hydrogen-bonding and noncovalent interactions. Despite these advantages, studies involving transition metal complexes with dimethylmalonate ligands are still relatively scarce, particularly in systems incorporating mixed ligand environments. The limited existing studies primarily involve metals such as Mn, Cu, Cd, Ba, Pt, U, Be, and Zn [2-9].

Moreover, the structural chemistry of metal-organic frameworks (MOFs) and complexes involving alkaline earth metals and dimethylmalonate ligands have been extensively studied, revealing the structural versatility and adaptability of these systems. For instance, a novel barium-dimethylmalonate MOF, $\{[Ba(C_5H_6O_4)(H_2O)]\cdot C_5H_8O_4\}_n$, was synthesized and structurally characterized, adding to the family of substituted malonate complexes with alkaline earth metals [10]. Similarly, a cadmium-dimethylmalonate MOF with a two-dimensional honeycomb structure and an extended hydrogen-bonded water network was reported, marking the first instance of such a water cluster in a cadmium-dimethylmalonate complex [11]. Earlier foundational work on the binding interactions of barium ions with various carboxylate ligands, including dimethylmalonate, provided critical insights that have informed subsequent MOF studies [12]. Similarly, transition metals such as Mn(II) have been explored for their potential to form luminescent and catalytically active complexes with dimethylmalonate [13]. Additionally, studies on the

spectroscopic analysis and synthesis of metal complexes of methyl malonate, often supported by computational methods, are limited but noteworthy [14, 15].

Additionally, noncovalent interactions such as hydrogen bonding and π–π stacking have been recognized as critical contributors to the stability and functionality of these complexes. These interactions not only influence crystal packing but also play a vital role in biological systems, such as stabilizing the structures of DNA [16] and RNA [17,18]. The application of 2,2'-bipyridine (Bpy) and its derivatives as secondary ligands is particularly valuable in assessing the aromatic residue stacking abilities within metal ion complexes involving carboxylic acids [19]. Understanding these forces within the context of Cu(II)-dimethylmalonate complexes can provide valuable insights into their potential biological and functional applications.

This study aims to address this gap by presenting a comprehensive investigation of the synthesis, spectroscopic characterization, crystal structure, and theoretical properties of a mixed ligand Cu(II) complex, $[Cu(Me_2mal)(bpy)(H_2O)]\cdot H_2O$. By combining experimental techniques such as single-crystal X-ray diffraction, IR, and UV-Vis spectroscopy with quantum mechanical methods like DFT and TD-DFT, this work provides a detailed understanding of the geometric, vibrational, and electronic properties of the complex. The interplay between hydrogen bonding and π–π interactions in the crystal packing, as well as their contribution to the overall stability and properties of the complex, is thoroughly examined.

Through this investigation, I'd like to contribute to the growing body of knowledge on mixed ligand Cu(II) complexes and highlight the potential of dimethylmalonate and bpy ligands in the design of multifunctional materials with promising structural and electronic properties.

## 2. Experimental and theoretical methods

### *2.1 Synthesis, materials and measurements*

The synthesis procedure involved dissolving $CuCl_2\cdot 2H_2O$ (1.452 g, 0.852 mmol) in 10 mL of water. An aqueous solution of dimethylmalonic acid (1.126 g, 0.852 mmol), 2,2'-bipyridine (1.31 g, 0.852 mmol) and NaOH (0.454 g, 1.7 mmol) in 60 mL of water was then added to the $CuCl_2\cdot 2H_2O$ solution. The reaction mixture was stirred at 70°C for 12 hours and then allowed to cool to room temperature. The precipitate formed in the mixture was then filtered and the resulting solution was allowed to evaporate slowly in the open air. After a few weeks, blue crystals suitable for X-ray diffraction studies precipitated.

Infrared (IR) spectra were collected in the 4000-400 $cm^{-1}$ range using a Perkin-Elmer Spectrum 100 FT-IR spectrometer, with the samples prepared as KBr pellets. Electronic absorption spectra were obtained by dissolving the compound (at a concentration of $10^{-3}$ M) in methanol, and the measurements were performed using a Shimadzu UV Mini-1240 UV-Vis spectrometer, covering the wavelength range of 200-450 nm.

### *2.2 Crystal data for the compounds*

X-ray diffraction data were obtained using the Bruker SMART BREEZE CCD diffractometer, which was purchased under the State Planning Organization grant number

2010K120480. To improve the accuracy of the collected data, absorption correction was applied using the multi-scan method and SADAPS V2012/1 software [20].

The structure of compound 1 was solved by direct methods using Olex2 [21] with SHELXS-97 and subsequently refined with SHELXL-97 [22]. The software packages Olex 2 and DIAMOND 3.0 (demo version) were used to obtain the molecular figures [23]. The refinement of all non-hydrogen atoms was carried out using the full matrix least squares method and was done anisotropically. Table 1 provides information on the data collection conditions and refinement process parameters.

Table 1. Crystal data and structure refinement of 1

| | |
|---|---|
| Empirical formula | 201.93 |
| Temperature/K | 296.15 |
| Crystal system | Orthorhombic |
| Space group | Pnnm |
| a/Å | 16.2662(14) |
| b/Å | 7.6693(7) |
| c/Å | 14.0101(12) |
| α/° | 90.00 |
| β/° | 90.00 |
| γ/° | 90.00 |
| Volume/Å$^3$ | 1747.8(3) |
| Z | 8 |
| $\rho_{calc}$ g/cm$^3$ | 1.535 |
| μ/mm$^{-1}$ | 1.289 |
| F(000) | 836.0 |
| Crystal size/mm$^3$ | 0.5 × 0.34 × 0.19 |
| Radiation | MoK$_\alpha$ (λ = 0.71073 Å) |
| 2Θ range for data collection/° | 3.84 to 56.88 |
| Index ranges | -21 ≤ h ≤ 21, -10 ≤ k ≤ 10, -18 ≤ l ≤ 18 |
| Reflections collected | 39401 |
| Independent reflections | 2297 [$R_{int}$ = 0.0253, $R_{sigma}$ = 0.0093] |
| Data/restraints/parameters | 2297/0/134 |
| Goodness-of-fit on F$^2$ | 1.119 |
| Final R indexes [I>=2σ (I)] | $R_1$ = 0.0271, $wR_2$ = 0.0741 |
| Final R indexes [all data] | $R_1$ = 0.0301, $wR_2$ = 0.0765 |
| H-atom treatment | H-atom parameters constrained |
| Largest diff. peak/hole / e Å$^{-3}$ | 0.33/-0.22 |

### *2.3 DFT Calculations*

The crystal structure of compound 1 provided the initial molecular geometry for subsequent computational investigations. Density Functional Theory (DFT) calculations were conducted at the B3LYP level, a widely recognized method known for its reliable alignment with experimental data [24, 25]. These calculations were performed using the GAUSSIAN 03 software package [26] and the resulting output files were visualized with GaussView 4.1 [27]. The molecular structure of the compound in its ground state was optimized using the B3LYP functional in conjunction with the 6-31G basis set. This same level of theory was applied to calculate the vibrational frequencies of the compound. To further refine the analysis, potential energy distribution (PED) calculations and the

assignment of fundamental vibrational modes were carried out using the VEDA4 program [28]. During the optimization process, no constraints were imposed on bond lengths, bond angles, or dihedral angles, allowing all atoms to freely adjust to their optimal positions. In addition, the electronic absorption spectrum was calculated by the LanL2DZ method using time-dependent density functional theory (TDDFT) [29]. Electronic absorption and emission spectra were calculated in methanol (MeOH) solution using the polarizable continuum model (PCM) [30]. These calculations were performed using the ground state geometry, previously optimized in the gas phase, as the initial geometry.

## 3. Results and discussions

### *3.1. Crystal structure of [Cu(Me$_2$mal)(bpy)(H$_2$O)]·H$_2$O*

Figure 1 displays the molecular structure of synthesized complex. Tables 1 and 2 present comprehensive crystallographic data, detailing the procedures for data collection and refinement, bond lengths, and angles, respectively.

X-ray diffraction analysis elucidates that complex 1 crystallizes within the orthorhombic space group Pnnm. The molecular structure of 1 shows that the Cu(II) ion is pentacoordinated, forming coordination bonds with two carboxylate oxygens from the dimethylmalonate dianion (L), two nitrogen atoms from bipyridine, and an axial water oxygen, visually depicted in Figure 1.

The structural arrangement surrounding the Copper (II) ion with five-coordination in complex 1 resembles that of previous studies, including [Cu(mal)(phen)(H$_2$O)]·1.5H$_2$O [31], [Cu3(mal)$_3$(phen)$_3$(H$_2$O)$_2$]·11H$_2$O [32] and [Cu(mal)(bipy)(H$_2$O)]·H$_2$O [33]. Both 2,2'-bipyridine and dimethylmalonate exhibit symmetric coordination within this coordination environment. The axial Cu1–O$_{water}$ bond measures 2.224 Å, which exceeds those of the Cu1–OMe$_2$mal (1.913 Å) and Cu1–N$_{bpy}$ (2.010 Å) bonds within the equatorial plane. This difference may be a result of the Jahn-Teller (JT) distortion, commonly observed in octahedral complexes of transition metal ions with $d^9$, $d^7$ (low-spin) and, $d^4$ (high-spin) electronic configurations [34-36]. Due to the $d^9$ electronic configuration of the Cu(II) ion, octahedral Cu(II) complexes exhibit a remarkable Jahn-Teller effect [37-40]. Additionally, it is acknowledged that a pseudo or second-order Jahn-Teller effect is apparent in pentacoordinated Cu(II) complexes. Depending on the ligand's nature and its coordinating atoms, two restricting geometries, specifically square pyramidal (SP) or trigonal bipyramidal (TBP), may be achieved [41, 42]. The trigonality index ($\tau$) serves as an informative metric for characterizing the coordination geometry surrounding the metal atom. It is calculated according to the equation $\tau = [|\theta - \varphi|/60]$, where $\theta$ and $\varphi$ indicate the largest coordination angles. The $\tau$ value varies from 0, which indicates a perfect square pyramidal geometry, to 1, which denotes a perfect trigonal bipyramidal arrangement [43]. In the analyzed structure, the inclusion of a chelating bpy ligand, malonate, and a coordinated water molecule culminates in a five-coordination environment around Cu(II), resulting in an almost perfect square pyramidal geometry ($\tau = 0$).

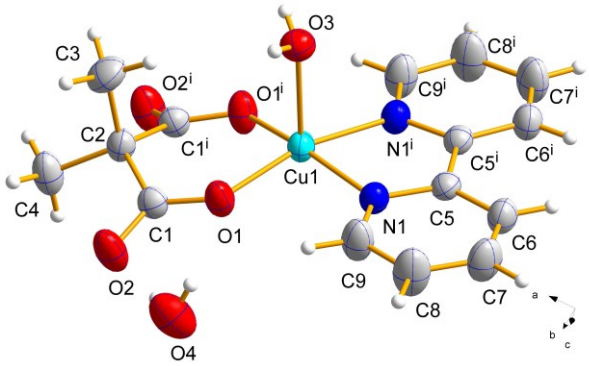


Figure 1. A view of symmetry related unit of titled compound (i: x, y, 1-z)

The planar arrangement that encompasses Cu1 comprises of two nitrogen (N1, $N1^{i}$) and two oxygen atoms from carboxyl (O1, $O1^{i}$), displaying an average deviation of 0.175(8) Å. Cu1 is placed 0.196(8) Å above the planar arrangement, pointing towards the apical oxygen atom (O2). The six-membered chelate ring formed by malonate in coordination with Cu1 adopts a boat conformation, details of which are given in Table 2.

Table 2. Comparison of selected bond lengths and angles.

| Parameters | X-Ray | Theoretical* |
|---|---|---|
| Bond Lengths (Å) | | |
| Cu1–O1 | 1.9128(11) | 1.916 |
| Cu1–$O1^{1}$ | 1.9129(11) | 1.880 |
| Cu1–O3 | 2.2249(16) | 2.455 |
| Cu1–N1 | 2.0097(13) | 2.008 |
| Cu1–$N1^{1}$ | 2.0097(13) | 1.999 |
| O1–C1 | 1.2708(18) | 1.337 |
| O2–C1 | 1.2383(19) | 1.244 |
| N1–C5 | 1.332(2) | 1.346 |
| N1–C9 | 1.3489(19) | 1.360 |
| C1–C2 | 1.5401(19) | 1.548 |
| C2–$C1^{1}$ | 1.5401(19) | 1.560 |
| C5–$C5^{1}$ | 1.478(3) | 1.479 |
| Angles (º) | | |
| $C(1)^{i}$—C(2)—C(1) | 114.61 (17) | 113.27 |
| N(1)—Cu(1)—$N(1)^{i}$ | 80.55 (7) | 80.556 |
| N(1)—Cu(1)—O(3) | 93.66 (5) | 107.70 |
| $N(1)^{i}$—Cu(1)—O(3) | 93.66 (5) | 86.538 |
| O(1)—Cu(1)—N(1) | 91.92 (5) | 91.377 |
| O(1)—Cu(1)—O(3) | 98.94 (5) | 111.854 |
| $O(1)^{i}$—Cu(1)—O(3) | 98.94 (5) | 71.950 |
| $O(1)^{i}$—Cu(1)—O(1) | 92.71 (5) | 94.960 |

Symmetry code: (i) *x, y, −z+1.*
**: B3LYP 631G*

Examination of the crystal packing shows that the complex is characterized exclusively by intermolecular hydrogen bonding of the O-H...O type, as shown in figure 2 and table 3.

Table 3. H-Bond interactions for the titled Cu(II) complex (Å).

| **D–H···A** | **D–H** | **H···A** | **D···A** | **D–H···A** |
|---|---|---|---|---|
| O3–H3…O4$^{i}$ | 0.77 (2) | 1.95 (2) | 2.717 (2) | 174 (2) |
| O4–H4D…O2$^{ii}$ | 0.74 (3) | 2.14 (3) | 2.878 (2) | 171 (3) |
| O4–H4E…O2 | 0.75 (4) | 2.10 (4) | 2.856 (2) | 180 (4) |
| Symmetry codes: (i) *−x+1/2, y−1/2, z−1/2*; (ii) *−x+1/2, y−1/2, −z+3/2*. | | | | |

A strong intermolecular hydrogen bond exists between the carboxylate oxygen atom O2 of dimethylmalonate and the uncoordinated water molecules. Additionally, hydrogen bond interactions occur between the coordinated and uncoordinated water molecules. These interactions lead to the formation of a molecular packing structure in the (100) plane.

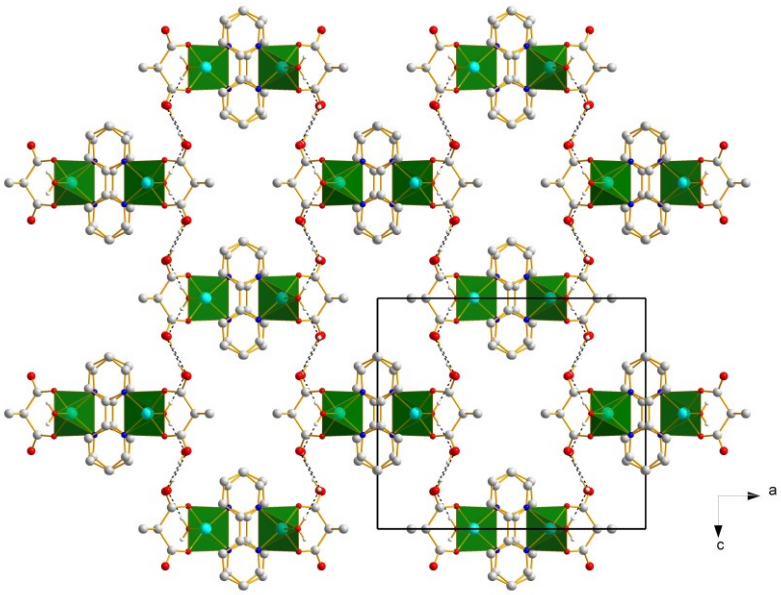


Figure 2. Packing of the Copper(II) complex along the b axis, with the H-bond interactions depicted as dashed lines.

Comprehensive analysis of the crystal packing for compound 1 reveals the presence of symmetrical face-to-face π–π stacking interactions between the pyridine rings of bpy, denoted as Ring 1 (Cg1): N1/C5/C6/C7/C8/C9 (as depicted in Figure 3). The interaction parameters are outlined below: the distances between the centroids of the rings and the ring centroid-to-plane distances between the pyridine rings measure 3.763(16) Å and 3.523(2) Å, correspondingly. These interactions between π orbitals lead to the creation of a polymeric structure along the b axis, which is one-dimensional (1D). Moreover, when these interactions (π–π stacking) combine with hydrogen bonding, they establish a packing framework that is three-dimensional framework.

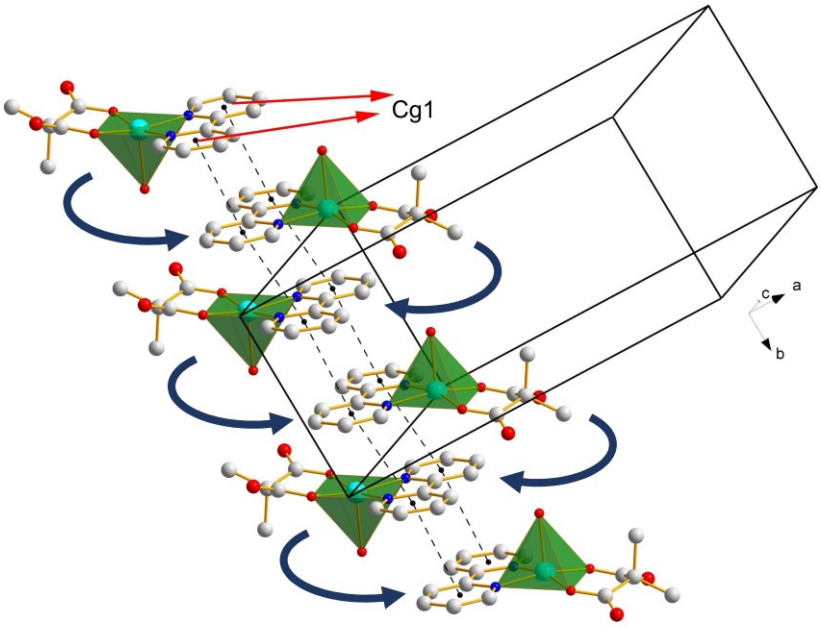


Figure 3. Illustrating π–π stacking interactions between the pyridine rings (shown as dashed lines), with H-atoms and free lattice water molecules omitted for clarity. (Cg 1: Ring centroid of N1-C5-C6-C7-C8-C9 atoms)

### *3.2 Optimized geometry and vibrational frequencies*

The geometry optimization of the titled complex was conducted utilizing the unrestricted hybrid density functional B3LYP/631G basis set. Table 2 provides a comparison of the calculated and experimental results. The theoretically computed values show an outstanding agreement with the X-ray diffraction data. Minor differences in bond lengths can be attributed to variations in conditions, as DFT calculations were carried out on an isolated molecule in the gaseous phase, whereas the X-ray crystallographic data were derived from the crystal lattice of complex molecules.

The results of the experiment suggest that the nitrogen atoms of bipyridine and the oxygen atoms of the carboxylate group are the most probable coordination sites. This conclusion is supported by the optimized structure's theoretical calculations. Notably, the $Me_2$mal group coordinates to the metal atom in a bidentate fashion, a fact confirmed by the theoretical methods, which reveal consistent Cu–O bond lengths, as presented in Table 2. The calculated Cu-N bond lengths in the complex align with standard values reported for Copper(II) complexes with bipyridine ligands, in accordance with earlier studies [44-47].

### *3.3. Infrared Spectroscopy*

Vibrational spectroscopy is a fundamental and versatile technique for the characterization of chemical compounds, effectively bridging experimental studies and theoretical calculations. Infrared (IR) spectroscopy enables the identification and assignment of specific vibrational modes within a molecule, a process that is significantly enhanced through the application of theoretical methods such as Density Functional Theory (DFT). Frequencies derived from DFT calculations provide precise and reliable references that facilitate the accurate differentiation of vibrational modes, especially in situations where IR absorption bands exhibit overlap. This synergistic use of experimental and

computational approaches ensures a more comprehensive understanding of molecular vibrational behavior and contributes to the detailed elucidation of chemical structures.
The comparison between calculated and experimental vibrations was conducted within the frequency range of 3700-600 $cm^{-1}$, Figure 4 shows the FT-IR spectrum for 1 in the 4000 to 400 $cm^{-1}$ frequency range. The FT-IR spectrum of 1 spans the frequency range from 4000 to 400 $cm^{-1}$, and it reveals bands that affirm the existence of all characteristic functional groups within the synthesized complex. In the IR spectrum of 1, a pronounced and wide band in the 3500–3200 $cm^{-1}$ region, associated with O–H stretching vibrations, signifies the presence of both coordinated and uncoordinated water molecules. The frequencies for this vibration were calculated to be 3664 and 3290 $cm^{-1}$. Glancing at table 4, the calculated frequencies for O–H stretching vibrations show a blue shift compared to the experimental IR data. Because of participating in hydrogen bonding, the experimental vibration frequencies of these groups were obtained at lower values.

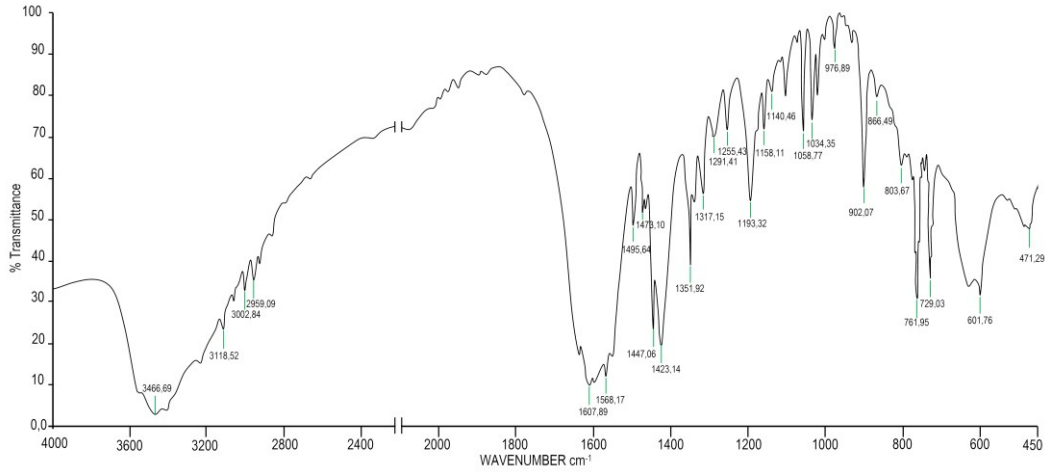


Figure 4. IR spectrum of reported copper (II) complex.

In characterizing the coordination modes of the carboxylate group, the difference between the asymmetric and symmetric carboxylate stretching frequencies [$\Delta\nu = \nu_{asym}(COO^{-}) - \nu_{sym}(COO^{-})$] provides valuable insights into the binding mode of the $COO^{-}$ moiety to the metal center, a method supported by previous research [48-52];

$\Delta\nu$ chelating < $\Delta\nu$ bridging < $\Delta\nu$ ionic < $\Delta\nu$ monodentate

When the value $\Delta\nu$ is below 250 $cm^{-1}$, the coordination is considered bidentate, while exceeding 250 $cm^{-1}$ indicates unidentate coordination of the carboxylate moiety. The synthesized complex has a calculated $\Delta\nu$ of 191 $cm^{-1}$, which strongly suggests the presence of bidentate coordination of carboxylate groups in the complex. This conclusion agrees with the X-ray diffraction data.
Furthermore, the malonate ion that is uncoordinated exhibits strong infrared bands at $\nu_{asym}(COO^{-})$ at 1698 $cm^{-1}$ and $\nu_{sym}(COO^{-})$ at 1434 $cm^{-1}$. The frequencies of these bands in the synthesized complex indicate a minor reduction.

Table 4. Experimental and DFT-B3LYP/6-31G calculated FT-IR spectra for $[Cu(Me_2mal)(bpy)(H_2O)]\cdot H_2O$ together with their assignment a (wavenumber in $cm^{-1}$).

| Exp. | Unscaled | Scaled | Assignment |
|---|---|---|---|
| 3466br | 3746 | 3664 | $\nu(OH)_{water}$ |
| 3234br | 3364 | 3290 | $\nu(OH)_{water}$ |
| 3118m | 3252 | 3180 | $\nu_s(CH)_{bipy.}$ |
| 3086m | 3235 | 3164 | $\nu_a(CH)_{bipy.}$ |
| 3027w | 3152 | 3083 | $\nu_a(CH_3)$ |
| 2959w | 3074 | 3006 | $\nu_s(CH_3)$ |
| 1615s | 1661 | 1624 | $\nu_a(OCO)$ |
| 1607s | 1655 | 1619 | $\nu(CC)_{bipy.}$, $\nu(CH)_{bipy.}$ |
| 1579s | 1620 | 1584 | $\nu(OH)_{water}$ |
| 1495m | 1515 | 1482 | $\nu(CH)_{bipy.}$, $\nu(CN)$ |
| 1473m | 1502 | 1469 | $\nu(CH)_{bipy.}$, $\nu(CN)$ |
| 1447s | 1479 | 1446 | $\rho(CH)_{bipy.}$ |
| 1424m | 1464 | 1432 | $\nu_s(OCO)$, $\nu(CH_3)$ |
| 1401m | 1437 | 1405 | $\nu(CH_3)$ |
| 1351m | 1325 | 1296 | $\nu_s(OCO)$, $\nu(CH)_{bipy.}$ |
| 1140w | 1169 | 1143 | $\nu(CO)$, $\nu(CH)_{bipy.}$, $\omega(CH_3)$ |
| 1074w | 1086 | 1062 | $\nu(CH)_{bipy.}$ |
| 1034w | 1057 | 1034 | $\nu(CH)_{bipy.}$ |
| 902m | 953 | 932 | $\omega(CH_3)$, $\nu(CCH_3)_{bipy.}$ |
| 866w | 887 | 867 | $\nu(CH_3)$, $\nu(OCO)$ |
| 761m | 800 | 782 | $\omega(CH)_{bipy.}$ |
| 743w | 768 | 751 | $\nu(CH)_{bipy.}$ |
| 729m | 754 | 737 | $\omega(OH)_{water}$ |
| 634w | 667 | 652 | $\nu(CuN)$ |
| 601w | 597 | 584 | $\nu(CuO)$ |

w = weak, m = medium, s = strong, br = broad, ν=stretching, ρ = in-plane rocking, δ = in-plane scissoring, ω = wagging, bipy. = 2,2'-bipyridine

The C=N stretching vibrations of the coordinated bpy molecule are responsible for the strong bands observed at 1495 and 1473 $cm^{-1}$. Theoretically calculated frequencies for C=N stretching at 1482 and 1469 $cm^{-1}$ agree well with experimental values. The $[Cu(Me_2mal)(bpy)(H_2O)]\cdot H_2O$ complex exhibits two bands at 634 and 601 $cm^{-1}$, corresponding to Cu–N and Cu–O vibrations, respectively. The experimental data calculated at 652 and 584 $cm^{-1}$, as shown in Table 4, strongly agrees with the computed values for these vibrations. In the $[Cu(Me_2mal)(bpy)(H_2O)]\cdot H_2O$ complex, two bands are observed at 634 and 601 $cm^{-1}$, which are comparable to the Cu-N and Cu-O vibrations, respectively. The computed frequencies for these vibrations, illustrated in Table 4, align well with the experimental data, determined at 652 and 584 $cm^{-1}$.

### *3.4. Electronic spectra and Natural bond orbital (NBO) analysis*

The UV-Vis spectrum of the titled complex in methanol has been recorded over a wavelength range of 200 - 450 nm (Fig 5). To further understand the electronic structure, the complex's electronic distribution has been theoretically investigated using the TD-B3LYP/LANL2DZ approach, and the results have been compared with experimental data. The determination of the energies of the Highest Occupied Molecular Orbital (HOMO), which acts as a π-donor, and Lowest The unoccupied molecular orbital (LUMO), also referred to as frontier molecular orbitals (FMOs), plays a crucial role in quantum chemical calculations. A key aspect of these investigations involves the determination of the energies of the Highest Occupied Molecular Orbital (HOMO) and the Lowest Unoccupied Molecular Orbital (LUMO), collectively referred to as frontier molecular orbitals (FMOs). These orbitals are pivotal in understanding the optical and electrical properties of the complex, as well as in analyzing its quantum chemistry and UV-Vis spectra [53]. The HOMO is typically associated with the electron-donating ability of a molecule, where a higher $E_{HOMO}$ value indicates a greater tendency to donate electrons. Conversely, the LUMO reflects the molecule's capacity to accept electrons, with lower $E_{LUMO}$ values indicating easier electron acceptance. The energy gap between the HOMO and LUMO levels ($\Delta E = E_{LUMO} - E_{HOMO}$) serves as a crucial stability index; smaller gaps suggest lower kinetic stability but higher chemical reactivity. Given their significance, both the experimental and theoretical results for these energy levels will be compared to enhance our understanding of the complex's properties [54-56].

Figures 5 and 6 show the experimental electronic spectra and isodensity plots for the HOMOs and LUMOs orbitals of the compound. Within the experimental spectrum of $[Cu(Me_2mal)(bpy)(H_2O)]\cdot H_2O$, four relatively intense absorption bands are observed in the 200–300 nm range. These bands are attributed to interligand transitions involving the π–bonding and π*–antibonding orbitals of the ligands. The peaks observed at 300 nm in experiments result from the transition of HOMO(B)→LUMO(B), with an energy of 4.13 eV. Other peaks detected at 291 nm and 240 nm in the same region are associated respectively with the transitions of HOMO–1(B)→LUMO(B) (energy of 4.51 eV) and HOMO–6(B)→LUMO(B) (energy of 5.26 eV).

Natural Bond Orbital (NBO) analysis is essential in determining key properties of molecules, such as their dipole moments, molecular polarizability, electronic structures, acidity, and basicity behaviors [57-61]. Additionally, NBO calculations offer valuable insights into the transfer of electrons between ligands and metal atoms.

Our study involved conducting NBO atomic charge calculations using the B3LYP/LANL2DZ basis set, with the outcomes outlined in Table 5. The results from this table display the electron densities within the Cu atom's 3d, 4s, and 4p orbitals as 9.15, 0.37, and 0.03 respectively. This highlights the noteworthy influence of Cu(II) atom’s 3d, 4s, and 4p orbitals in coordinating with N1, O1, and O3 atoms.

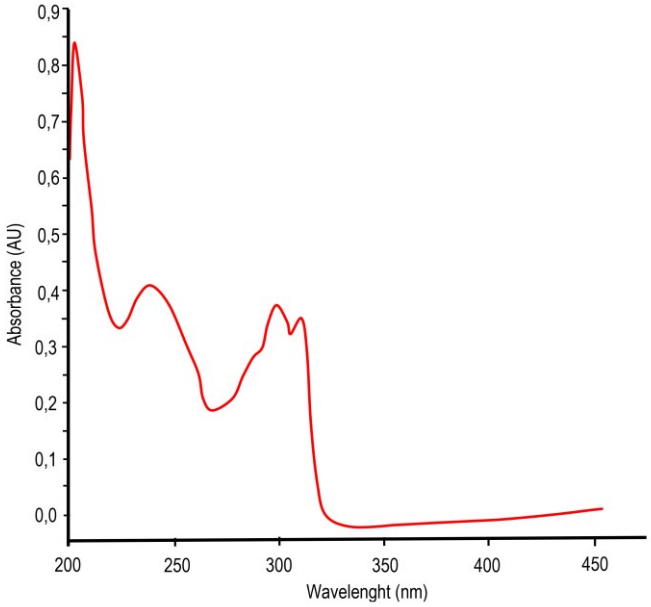


Figure 5. The compound's absorption spectrum ranges from 200 to 450 nm.

The analysis of electron distributions in the orbitals of N1, O1 and O3 atoms shows that the Cu atom coordinates with these atoms mainly using their 2s and 2p orbitals, as confirmed by Table 5. Therefore, the calculated neutral charge of the Cu atom in the complex is +1.43, which is lower than the formal charge of +2, suggesting that the ligands transfer charge to the Cu(II) ion. Additionally, the theoretical calculations indicate that the oxygen atoms O1 (-0.89) and O3 (-1.01) within the Copper(II) complex carry the most significant negative charges.

Table 5. Some of the natural atomic charges and electronic configurations for the coordination of copper (II).

| Atoms | Net charge | Electronic Configuration |
|---|---|---|
| Cu(1) | 1.43780 | [core]4S(0.37)3d( 9.15)4p( 0.03)5p( 0.01) |
| N(1) | -0.57583 | [core]2S(1.34)2p( 4.21)3p( 0.02) |
| O(1) | -0.89657 | [core]2S(1.73)2p( 5.16)3p( 0.01) |
| O(3) | -1.01703 | [core]2S(1.76)2p( 5.25)3p( 0.01)3d( 0.01) |

NBO analysis enables the evaluation of electron density distribution between Lewis-type orbitals that are occupied and non-Lewis NBOs that are formally unoccupied, indicating a stabilizing donor-acceptor interplay [62]. Second-order perturbation theory can be employed to anticipate the strength of the donor-acceptor interaction. In this context, the NBO analysis reveals the localization of lone pairs on the O and N atoms within the complex, as shown by the calculated second-order interaction energies (E2).

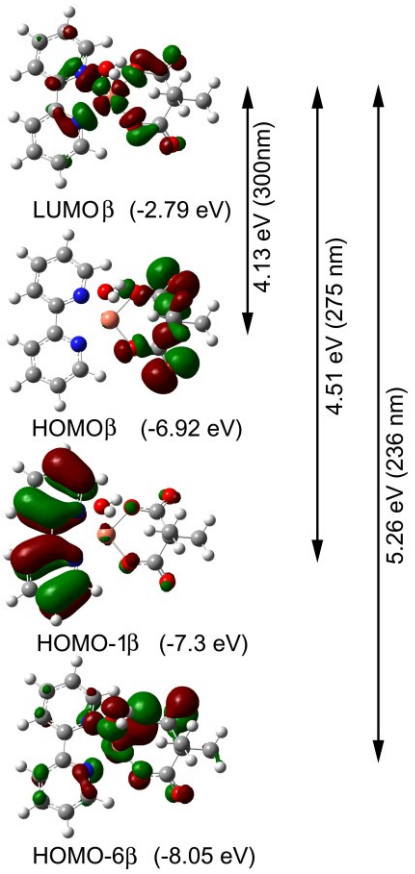


Figure 6. The isodensity plots for the HOMOs and LUMOs orbitals of the compound.

Specifically, the N1, O1, and O3 atoms exhibit calculated second-order interaction energies of 15.92 kcal/mol, 19.52 kcal/mol and 2.22 kcal/mol respectively. These values correspond to the strength of the metal-ligand bond lengths in the complex [O(1)-Cu(1): 1.913 Å, N(1)-Cu(1): 2.009 Å, O(3)-Cu(1): 2.224 Å].

## 4. Conclusions

In this study, a novel Cu(II) complex was synthesized using dimethylmalonate dianion and 2,2'-bipyridine ligands and analyzed through a combination of IR, UV-Vis spectroscopy, and X-ray diffraction techniques. The X-ray crystallographic analysis of the [Cu($Me_2$mal)(bpy)($H_2O$)]·$H_2O$ complex revealed that the Cu(II) ion is coordinated by the dimethylmalonate and 2,2'-bipyridine ligands in a bidentate fashion, with an oxygen atom from a water molecule occupying the axial position. The coordination environment, characterized by Jahn-Teller distortion, results in an almost perfect square pyramidal geometry, as confirmed by a trigonality index (τ) value of 0.

Furthermore, a careful study of the intermolecular interactions revealed that, in addition to hydrogen bonding, π–π stacking interactions play a crucial role in the three-dimensional packing of the crystal structure.

The combined experimental and theoretical approaches provide a detailed understanding of the bonding and structural characteristics of the complex. Density Functional Theory

(DFT) calculations show excellent agreement with experimental X-ray diffraction data, affirming the reliability of the theoretical model.

The electronic and vibrational properties of the complex were further explored through theoretical calculations, which closely matched the experimental vibrational frequencies, underscoring the robustness of the employed methodology. Infrared spectroscopy confirmed the bidentate coordination of the $Me_2mal$ ligand, as evidenced by the $\Delta\nu$ value of 191 $cm^{-1}$, in alignment with the X-ray findings. Time-Dependent DFT (TD-DFT) calculations showed high concordance with the experimental absorption spectra in methanol, elucidating the electronic transitions predominantly occurring between the $\pi$-bonding and $\pi^*$-antibonding orbitals of the ligands.

The NBO analysis of the titled complex provided valuable insights into the stabilization energies as deduced from the second-order perturbation energies, which were remarkably minimal. Natural Bond Orbital (NBO) analysis reveals significant charge transfer from the ligands to the Cu(II) ion, with the Cu atom exhibiting a reduced formal charge of +1.43. The calculated second-order interaction energies further underscore the stability of the metal-ligand bonds within the complex.

In conclusion, the $[Cu(Me_2mal)(bpy)(H_2O)]\cdot H_2O$ complex demonstrates a well-defined crystal structure with significant electronic interactions, offering valuable insights into the coordination chemistry of Cu(II) complexes. The synergy between experimental data and theoretical calculations enhances our understanding of its structural and electronic properties, contributing to the broader field of coordination chemistry. I also believe that this comprehensive study will serve as a valuable resource for improving our understanding of the spectroscopic behavior of coordination compounds involving malonates.

## Supporting information

CCDC1403346 contains supplementary crystallographic data for synthesized complex. These data can be obtained free of charge from The Cambridge Crystallographic Data Centre via www.ccdc.cam.ac.uk/data_request/cif.

## References

[1] Pasán, J., Delgado, F.S., Rodríguez-Martín, Y., Hernández-Molina, M., Ruiz-Pérez, C., Sanchiz, J., Lloret, F., Julve, M., Malonate-based copper(II) coordination compounds: ferromagnetic coupling controlled by dicarboxylates, **Polyhedron** 22, 2143-2153 (and references therein), (2003).

[2] Alderighi, L., Cecconi, F., Ghilardi, C. A., Mederos, A., Midollini, S., Orlandini, A. and Vacca, A., Complexes of beryllium(II) with substituted malonates. Crystal structure of $K_2[Be(C_4H_6(COO)_2)_2]\cdot 2H_2O$. **Polyhedron**, 18, 3305-3312, (1999).

[3] Deniz, M., Hernandez-Rodriguez, I., Pasan, J., Fabelo, O., Canadillas-Delgado, L., Yuste, C., Julve, M., Lloret, F. and Ruiz-Perez, C., Pillaring Role of 4,4′-Azobis(pyridine) in Substituted Malonate-Containing Manganese(II) Complexes: Syntheses, Crystal Structures, and Magnetic Properties. **Crystal Growth & Design** 12, 4505-4518, (2012).

[4] Farnum, G. A., Nettleman, J. H. and LaDuca, R. L., Structure and physical properties of substituted malonate divalent metal coordination polymers with dipyridylamine co-ligands: acentric chain, herringbone layer, and novel binodal network topologies. **Crystengcomm**, **12**, 888-897, (2010).

[5] Guo, M.-L. and Wang, F.-Q., Poly[diaquabis([μ]$_3$-2,2dimethylpropanedioato) calcium(II)copper(II)] **Acta Crystallographica Section C-Crystal Structure Communications, 66**, M184-M187, (2010a).

[6] Guo, M.-L. and Wang, F.-Q., Poly [[aqua-$\mu_3$-2, 2-dimethylmalonato-copper (II)] monohydrate] and poly [aqua-$\mu_3$-2,2-dimethylmalonato-copper(II)]. **Acta Crystallographica Section C-Crystal Structure Communications, 66**, M379-M383, (2010b).

[7] Guo, M.-L. and Zhao, Y.-N., Poly [aqua-$\mu_3$-2,2-dimethylmalonato-zinc(II)]. **Acta Crystallographica Section C-Crystal Structure Communications, 62,** M563-M565, (2006).

[8] Mukhopadhyay, U., Thurston, J. H., Whitmire, K. H. and Khokhar, A. R., Synthesis and characterization of cis-bis-heptamethyleneimine platinum(II) dicarboxylate complexes: crystal structure of cis-[Pt(heptamethyleneimine)$_2$(malonate)]·$H_2O$. **Polyhedron**, **21**, 2369-2374, (2002).

[9] Zhang, Y. J., Livens, F. R., Collison, D., Helliwell, M., Heatley, F., Powell, A. K., Wocadlo, S. and Eccles, H., Synthesis and characterisation of uranyl substituted malonato complexes: Part I. Structural diversity with dimethylmalonate and different counter-cations. **Polyhedron**, **21**, 69-79, (2002).

[10] Guo, M.-L. and Guo, C.-H., Poly[[aqua-([m]-2,2-dimethyl-malonato)-barium(II)] 2,2-dimethyl-malonic acid solvate]. **Acta Crystallographica Section C-Crystal Structure Communications, 64**, M398-M400, (2008).

[11] Guo, M.-L. and Guo, C.-H., Poly[[diaqua-([m]$_3$-2,2-dimethyl-malonato)-cadmium(II)] tetra-hydrate**]. Acta Crystallographica Section C-Crystal Structure Communications, 65**, M266-M268, (2009).

[12] Yoshinobu Yokomori, Y., Flaherty, K. A., Hodgson, D. J., Barium binding to .gamma.-carboxyglutamate and .beta.-carboxyaspartate residues: structures of barium complexes of benzylmalonate, dimethylmalonate, and ethylmalonate ions. **Inorg. Chem.** 27, 13, 2300–2306, (1998).

[13] Deniz, M., Hernandez-Rodriguez, I., Pasan, J., Fabelo, O., Canadillas-Delgado, L., Vallejo, J., Julve, M., Lloret, F. and Ruiz-Perez, C., Syntheses, crystal structures and magnetic properties of five new Manganese(II) complexes: influence of the conformation of different alkyl/aryl substituted malonate ligands on the crystal packing. **Crystengcomm**, **16**, 2766-2778, (2014).

[14] Drommi, D., Saporita, M., Bruno, G., Faraone, F., Scafato, P. and Rosini, C., Origin of enantioselectivity in palladium-catalyzed asymmetric allylic alkylation reactions using chiral N, N-ligands with different rigidity and flexibility**. Dalton Transactions**, **15**, 1509-1519, (2007).

[15] Schmeier, T. J., Nova, A., Hazari, N. and Maseras, F., Synthesis of PCP-Supported Nickel Complexes and their Reactivity with Carbon Dioxide. **Chemistry-a European Journal, 18**, 6915-6927, (2012).

[16] Saenger, W., Defining Terms for the Nucleic Acids. In: Principles of Nucleic Acid Structure. **Springer Advanced Texts in Chemistry.** Springer, New York, pp 9-28, (1984).

[17] Sigel, R. K., and Pyle, A. M., Alternative roles for metal ions in enzyme catalysis and the implications for ribozyme chemistry. **Chemical reviews, 107(1)**, 97-113, (2007).

[18] Erat, M. C., Zerbe, O., Fox, T., and Sigel, R. K., Solution structure of domain 6 from a self-splicing group II intron ribozyme: A $Mg^{2+}$ binding site is located close to the stacked branch adenosine. **ChemBioChem, 8(3)**, 306-314, (2007).

[19] Yamauchi, O., Odani, A., Masuda, H., & Sigel, H., Stacking interactions involving nucleotides and metal ion complexes. **Metal Ions in Biological Systems**, **32**, 207-270, (1996).

[20] Bruker, SADABS, Bruker AXS Inc., Madison, WI, (2005).

[21] Dolomanov, O. V., Bourhis, L. J., Gildea, R. J., Howard, J. A., & Puschmann, H., OLEX2: a complete structure solution, refinement and analysis program. **Journal of applied crystallography**, **42(2)**, 339-341, (2009).

[22] Sheldrick, G. M., SHELX-97–Programs for crystal structure determination (SHELXS) and refinement (SHELXL). **Acta Crystallogr. A**, 64, 112, (2008).

[23] Brandenburg, K., DIAMOND Demonstrated Version, **Crystal Impact GbR**. Bonn, Germany, (2005).

[24] Becke, A. D., Density-functional thermochemistry. III. The role of exact exchange. **The Journal of Chemical Physics**, 98 (7), 5648–5652, (1993).

[25] Lee, C., Yang, W. and Parr, R.G., Development of the Colle-Salvetti Correlation-Energy Formula into a Functional of the Electron Density. Physical Review B, **37**, 785-789, (1988).

[26] Frisch, M. J.; Trucks, G. W.; Schlegel, H. B.; Scuseria, G. E.; Robb, M. A.; Cheeseman, J. R.; Montgomery, Jr., J. A.; Vreven, T.; Kudin, K. N.; Burant, J. C.; Millam, J. M.; Iyengar, S. S.; Tomasi, J.; Barone, V.; Mennucci, B.; Cossi, M.; Scalmani, G.; Rega, N.; Petersson, G. A.; Nakatsuji, H.; Hada, M.; Ehara, M.; Toyota, K.; Fukuda, R.; Hasegawa, J.; Ishida, M.; Nakajima, T.; Honda, Y.; Kitao, O.; Nakai, H.; Klene, M.; Li, X.; Knox, J. E.; Hratchian, H. P.; Cross, J. B.; Bakken, V.; Adamo, C.; Jaramillo, J.; Gomperts, R.; Stratmann, R. E.; Yazyev, O.; Austin, A. J.; Cammi, R.; Pomelli, C.; Ochterski, J. W.; Ayala, P. Y.; Morokuma, K.; Voth, G. A.; Salvador, P.; Dannenberg, J. J.; Zakrzewski, V. G.; Dapprich, S.; Daniels, A. D.; Strain, M. C.; Farkas, O.; Malick, D. K.; Rabuck, A. D.; Raghavachari, K.; Foresman, J. B.; Ortiz, J. V.; Cui, Q.; Baboul, A. G.; Clifford, S.; Cioslowski, J.; Stefanov, B. B.; Liu, G.; Liashenko, A.; Piskorz, P.; Komaromi, I.; Martin, R. L.; Fox, D. J.; Keith, T.; Al-Laham, M. A.; Peng, C. Y.; Nanayakkara, A.; Challacombe, M.; Gill, P. M. W.; Johnson, B.; Chen, W.; Wong, M. W.; Gonzalez, C.; and Pople, J. A., Gaussian 03, Revision **C.02**, Gaussian, Inc., Wallingford CT, (2004).

[27] Frisch, A., Dennington, I. I. R., Keith, T., Millam, J., Nielsen, A. B., Holder, A. J., and Hiscocks, J., Version **4.0**, Gaussian Inc, (2007).

[28] Jamroz, M. H., Vibrational energy distribution analysis. VEDA 4, Warsaw, (2004).

[29] Gross, E. K. U., and Kohn, W., Local density-functional theory of frequency-dependent linear response. **Physical review letters**, **55(26)**, 2850-2852, (1985).

[30] Caricato, M., Mennucci, B., Tomasi, J., Ingrosso, F., Cammi, R., Corni, S., and Scalmani, G., Formation and relaxation of excited states in solution: A new time dependent polarizable continuum model based on time dependent density functional theory. **The Journal of chemical physics, 124(12)**, 124520, (2006).

[31] Kwik, W. L., Ang, K. P., Chan, H. S. O., Chebolu, V., and Koch, S. A., Thermal, spectroscopic, and structural properties of aqua (malonato-O,O′)(1,10-

phenanthroline) Copper (II) hydrate (1/1.5). **Journal of the Chemical Society, Dalton Transactions, (12)**, 2519-2523, (1986).

[32] Zhang, Q.-Z., Lu, C.-Z., and Yang, W.-B., Synthesis and crystal structure of a Cu(II) complex with mixed malonate/1,10-phenanthroline ligands. **Journal of Coordination Chemistry, 58:18**, 1759-1764, (2005).

[33] Shen, H. Y., Bu, W. M., Liao, D. Z., Jiang, Z. H., Yan, S. P., and Wang, G. L., A new mixed-ligand one dimensional complex via hydrogen bonds: Cu (Mal)(bpy)· $2H_2O$ (Mal= Malonate ion, bpy= 2, 2′-bipyridine). **Inorganic Chemistry Communications, 3(9)**, 497-500, (2000).

[34] I.B. Bersuker (Ed.), The Jahn–Teller Effect, **Cambridge University Press**, Cambridge, p. 609, (2006).

[35] Jahn, H. A. and Teller, E., Stability of polyatomic molecules in degenerate electronic states-I—Orbital degeneracy. Proceedings of the Royal Society of London. **Series A-Mathematical and Physical Sciences, 161(905)**, 220-235, (1937).

[36] Jahn, H. A., Stability of polyatomic molecules in degenerate electronic states II-Spin degeneracy. Proceedings of the Royal Society of London. **Series A-Mathematical and Physical Sciences**, 164(916), 117-131, (1938).

[37] Moore, E. A. and Janes, R., Metal-Ligand Bonding. **Royal Society of Chemistry**, p. 108, (2007).

[38] B. J. Hathaway, Structure and Bonding, **57**, **Springer Verlag**, New York-Berlin-Heidelberg, p. 56, (1984).

[39] Veidis, M. V., Schreiber, G. H., Gough, T. E., and Palenik, G. J., Jahn-Teller distortions in octahedral copper (II) complexes. **Journal of the American Chemical Society**, **91(7),** 1859-1860, (1969).

[40] Belicchi, M. F., Gasparri, G. F., Pelizzi, C., and Tarasconi, P., Synthesis and X-ray structures of dinitrato-bis [2-(2′-thienyl)-1-(2′-thienylmethyl) benzimidazole] copper (II) and dichloro-bis-[2-(2′-thienyl)-benzimidazole] copper (II)-ethanol. **Transition Metal Chemistry**, **10(8)**, 295-299, (1985).

[41] Pearson, R. G., Concerning jahn-teller effects. **Proceedings of the National Academy of Sciences, 72(6)**, 2104-2106, (1975).

[42] Reinen, D., and Atanasov, M., Fluxionality and stereochemistry of 5-coordinate Cu2+ complexes. The potential energy surface and spectroscopic implications. **Chemical physics, 136(1)**, 27-46, (1989).

[43] Addison, A. W., Rao, T. N., Reedijk, J., van Rijn, J., and Verschoor, G. C., Synthesis, structure, and spectroscopic properties of copper (II) compounds containing nitrogen–sulphur donor ligands; the crystal and molecular structure of aqua [1, 7-bis (N-methylbenzimidazol-2′-yl)-2, 6-dithiaheptane] copper (II) perchlorate. **Journal of the Chemical Society, Dalton Transactions, (7)**, 1349-1356, (1984).

[44] Kočanová, I., Kuchár, J., Orendáč, M. and Černák, J., Cu–Ni heterobimetallic compounds. Part 2: Study of the system Cu(II)–bpy–$[Ni(CN)_4]$ 2−(bpy= 2, 2′-bipyridine). **Polyhedron**, **29(18**), 3372-3379, (2010).

[45] Ferlay, S., Francese, G., Schmalle, H. W. and Decurtins, S., A new bidimensional compound containing (μ-thiocyanate)(bpy) copper(II) molecules: synthesis, crystal structure and magnetic properties of $[Cu(bpy)(NCS)_2]_n$ (bpy=2,2′-bipyridyl). **Inorganica chimica acta, 286(1),** 108-113, (1999).

[46] Phuengphai, P., Youngme, S., Chaichit, N., Pakawatchai, C., van Albada, G. A., Quesada, M. and Reedijk, J., Crystal structures and magnetic properties of two new phosphate-metal complexes: [Cu2 (bpy) 2 (μ, $\eta_2$-$HPO_4$)(μ, $\eta_1$-$H_2PO_4$)(μ, $\eta_2$-

$H_2PO_4$)] n and [Cu4 (phen)$_4$ ($\mu_3$, $\eta_2$-$HPO_4$)$_2$ ($\mu$, $\eta_2$-$H_2PO_4$) 2($H_2PO_4$)$_2$]($H_2O$)$_4$. **Polyhedron**, **25(11)**, 2198-2206, (2006).

[47] Youngme, S., Chaichit, N., Pakawatchai, C. and Booncoon, S., The coordination chemistry of mono and bis(di-2-pyridylamine) copper(II) complexes: preparation, characterization and crystal structures of [Cu(L)($NO_2$)$_2$],[Cu (L)($H_2O$)$_2$($SO_4$)],[Cu(L)$_2$(NCS)](SCN)·0.5DMSO and [Cu(L)$_2$(SCN)$_2$]. **Polyhedron**, **21(12-13)**, 1279-1288, (2002).

[48] Kumar, U., Thomas, J., Nagarajan, R. and Thirupathi, N., 3, 5-Lutidine coordinated zinc (II) aryl carboxylate complexes: Precursors for zinc (II) oxide. **Inorganica Chimica Acta, 372(1)**, 191-199, (2011).

[49] Mehrotra R. C. and Bohra, R., Metal Carboxylates, **Academic Press**, New York, p. 396, (1983).

[50] Deacon, G. B. and Phillips, R. J., 1980. Relationships between the carbon-oxygen stretching frequencies of carboxylato complexes and the type of carboxylate coordination**. Coordination chemistry reviews, 33(3)**, 227-250, (1983).

[51] Nakamoto, K., Infrared and Raman Spectra of Inorganic and Coordination Compounds: Theory and Applications in Inorganic Chemistry, 5th ed.; **John Wiley & Sons:** New York, p. 350, (1997).

[52] Zeleňák, V., Vargová, Z. and Györyová, K., Correlation of infrared spectra of zinc (II) carboxylates with their structures. **Spectrochimica Acta Part A: Molecular and Biomolecular Spectroscopy, 66(2)**, 262-272, (2007).

[53] Fleming, I., Frontier Orbitals and Organic Chemical Reactions, **John Wiley & Sons**, New York, p. 249, (1976).

[54] Obot, I. B., Obi-Egbedi, N. O., Eseola, A.O., Anticorrosion Potential of 2-Mesityl-1H-imidazo[4,5-f][1,10]phenanthroline on Mild Steel in Sulfuric Acid Solution: Experimental and Theoretical Study, **Industrial & Engineering Chemistry Research,** 50, 2098, (2011).

[55] Obot, I. B., Obi-Egbedi, N. O., Theoretical study of benzimidazole and its derivatives and their potential activity as corrosion inhibitors, **Corrosion Science**, Volume 52, Issue 2, Pages 657-660, (2010).

[56] Obreedot, I. B. and Obi-Egbedi, N. O., Anti-corrosive properties of xanthone on mild steel corrosion in sulphuric acid: Experimental and theoretical investigations, **Current Applied Physics**, Volume 11, Issue 3, Pages 382-392, (2011)

[57] Foster, A. J. and Weinhold, F., Natural hybrid orbitals. **Journal of the American Chemical Society**, **102(24)**, 7211-7218, (1980).

[58] Reed, A. E. and Weinhold, F., Natural bond orbital analysis of near-Hartree–Fock water dimer. **The Journal of Chemical Physics, 78(6)**, 4066-4073, (1983).

[59] Reed, A. E., Weinstock, R. B., and Weinhold, F., Natural population analysis**. The Journal of Chemical Physics**, 83(2), 735-746, (1985).

[60] Reed, A. E. and Weinhold, F., Natural localized molecular orbitals. **The Journal of Chemical Physics**, **83(4)**, 1736-1740, (1985).

[61] Carpenter, J. E. and Weinhold, F., Analysis of the geometry of the hydroxymethyl radical by the "different hybrids for different spins" natural bond orbital procedure. **Journal of Molecular Structure: THEOCHEM, 169**, 41-62, (1988).

[62] Reed, A. E., Curtiss, L. A. and Weinhold, F., Intermolecular interactions from a natural bond orbital, donor-acceptor viewpoint. **Chemical Reviews, 88(6)**, 899-926, (1988).